Frequency-Domain Oversampling for Zero-Padded OFDM in Underwater Acoustic Communications

Zhaohui Wang, *Student Member, IEEE,* Shengli Zhou, *Member, IEEE,* Georgios B. Giannakis, *Fellow, IEEE*, Christian R. Berger, *Member, IEEE*, and Jie Huang

This work is supported by the ONR grants N00014-07-1-0805 (YIP), N00014-09-1-0704 (PECASE), and the NSF grant CNS-0721834.

Z-H. Wang, S. Zhou, and J. Huang are with the Department of Electrical and Computer Engineering, University of Connecticut, 371 Fairfield Way U-2157, Storrs, CT 06269, USA (email: {zhwang, shengli, jhuang}@engr.uconn.edu).

G. B. Giannakis is with the Department of Electrical and Computer Engineering, University of Minnesota, 200 Union Street SE, Minneapolis, MN 55455, USA (email: georgios@ece.umn.edu).

C. R. Berger is with the Department of Electrical and Computer Engineering, Carnegie Mellon University, 5000 Forbes Avenue, Pittsburgh, PA 15213, USA (email: crberger@ece.cmu.edu).

Contact author: Z-H. Wang, Tel.: (860) 617-4412, email: zhwang@engr.uconn.edu

Abstract

Although time-domain oversampling of the received baseband signal is common for single-carrier transmissions, the counterpart of frequency-domain oversampling is rarely used for multicarrier transmissions. This is because frequency-domain oversampling cannot be taken advantage of, when using the commonly used low-complexity receiver that assumes orthogonal subcarriers. In this paper, we explore frequency-domain oversampling to improve the system performance of zero-padded orthogonal frequency division multiplexing transmissions over underwater acoustic channels with large Doppler spread. On these channels intercarrier interference has to be addressed explicitly via frequency domain equalization, which enables inclusion of additional frequency samples at little increased complexity. We use a signal design that enables separate sparse channel estimation and data detection, reducing equalization complexity. Based on both simulation and experimental results, we observe that the receiver with frequency-domain oversampling outperforms the conventional one considerably, where the gain increases as the Doppler spread increases.

Index Terms

OFDM, zero-padding, intercarrier interference, Doppler spread, frequency-domain oversampling.

I. Introduction

Recently, zero-padded (ZP) orthogonal frequency division multiplexing (OFDM) has been extensively investigated for high data rate underwater acoustic communications [1]–[3]. Following Doppler shift compensation and an overlap-add operation, fast Fourier transform (FFT) is performed on the received block to obtain frequency-domain samples, that are used for subsequent channel estimation and data detection [1]–[3]. However, overlap-adding incurs information loss: it folds a received block that is a linear convolution of the input and the channel, into a *shorter* block that corresponds to a circular convolution of the input with the channel. This fact has been recognized in [4], and alternative receivers have been developed to improve system performance.

In spite of its known suboptimality, the overlap-add operation is used in most ZP-OFDM receivers. This is because on channels that are linear, time-invariant, or can be approximated as such after proper processing [1], [2], the overlap-add operation preserves the orthogonality among subcarriers, which enables low-complexity equalization and demodulation. This is no longer the case on strongly time-varying channels [3], where intercarrier interference (ICI) impairs subcarrier orthogonality, thus requiring adjacent subcarriers to be jointly demodulated.

In this paper, we investigate the use of frequency-domain oversampling for ZP-OFDM to improve system performance over underwater acoustic channels with large Doppler spread. At the outset, this paper distinguishes itself from [4] in the following aspects: (i) The receivers in [4] are based on a time-invariant channel, while this paper considers time-varying channels with large Doppler spread; (ii) The receivers in [4] assume perfect channel knowledge, while this paper deals with both channel estimation and data detection; (iii) The performance results in [4] are based on simulations only, where the FFT block sizes are considerably smaller than those used in practical systems. This paper validates the system performance using real data collected from field experiments.

We consider the same ZP-OFDM signal design as in [5], [6] that separates data subcarriers from pilot subcarriers using interspersed null subcarriers. This way, channel estimation and data detection can be carried out separately at the receiver, even in channels with large Doppler spread. We further develop a frequency-domain oversampling receiver, that relies on compressed sensing techniques for sparse channel estimation and minimum mean-square error (MMSE) equalization for data detection. The receiver complexity is only increased marginally by the frequency-domain oversampling: the FFT size increases proportionally and the equalizers process more inputs – *but* the equalizer complexity is dominated by the matrix inversion which scales with the number of data symbols – not the observations. In addition to the rectangular pulse-shaping window, we also consider raised-cosine windows in the signal design to further alleviate the ICI.

We evaluate the performance of the proposed receiver using both simulated and real data collected from the SPACE08 experiment, conducted off the coast of Martha's Vineyard, Massachusetts, October 2008, and the WHOI09 experiment, conducted in the Buzzards Bay, Massachusetts, December 2009. Simulation results demonstrate that frequency-domain oversampling improves the system performance considerably, where the performance gain increases as the channel Doppler spread increases. Experimental results verify the benefits of frequency-domain oversampling in achieving similar performance with fewer phones than the receiver without oversampling. Interestingly, although a raised-cosine pulse-shaping window improves performance relative to a rectangular window, the performance gain is less pronounced when using frequency-domain oversampling.

Note that time-domain oversampling is commonly used for single-carrier transmissions [7]. Its dual, the frequency-domain oversampling method, is rarely used for multicarrrier transmissions.

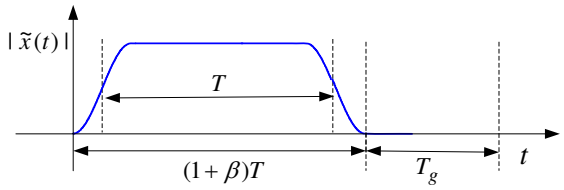

(a) One transmitted ZP-OFDM block

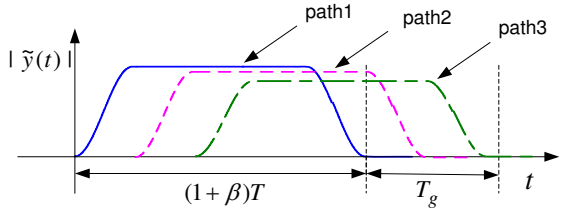

(b) One received ZP-OFDM block

Fig. 1. Illustration of the transmitted and received signals in the time domain.

So far, we are only aware of [8], where frequency-domain oversampling has been employed in the context of blind carrier-frequency-offset recovery for OFDM systems. Certainly, frequency-domain processing can also be used for single-carrier transmissions, see e.g., [9]. However, frequency-domain oversampling has not been considered therein.

The contribution of this paper lies in providing concrete evidence to demonstrate the benefit of frequency-domain oversampling in practical systems. This study could motivate further research on frequency-domain oversampling in other scenarios.

The rest of the paper is organized as follows. The system model is introduced in Section II. The proposed transmitter and receiver designs are presented in Section III. Numerical simulations are given in Section IV, and experimental results are collected in Sections V and VI. We conclude in Section VII.

Notation: Bold upper-case and lower-case letters denote matrices and column vectors, respectively; $(\cdot)^T$, $(\cdot)^*$, and $(\cdot)^H$ denote transpose, conjugate, and Hermitian transpose, respectively. $\mathbf{I}_N$ stands for an identity matrix with size N.

II. System Model And Motivation

Zero-padded OFDM with rectangular pulse-shaping windows has been used in [1]–[3]. In this paper, we also consider raised-cosine pulse-shaping windows. With T denoting the symbol

duration, and β denoting the roll-off factor, the raised-cosine window is [7]

$$g(t) = \begin{cases} 1, & t \in \left[\frac{\beta}{2}T, T\right] \\ \frac{1}{2}\left[1 + \cos\left(\frac{\pi}{\beta T}\left(\left|t - \frac{1+\beta}{2}T\right| - \frac{1-\beta}{2}T\right)\right)\right], & t \in \left[0, \frac{\beta}{2}T\right) \cup (T, (1+\beta)T] \\ 0, & \text{otherwise} \end{cases} \quad (1)$$

whose Fourier transform is

$$G(f) = \frac{\sin(\pi f T)}{\pi f T} \cdot \frac{\cos(\pi \beta f T)}{1 - 4\beta^2 f^2 T^2} e^{-j\pi f(1+\beta)T}. \quad (2)$$

When $\beta = 0$, $g(t)$ in (1) reduces to the rectangular window used in [1]–[3].

With symbol duration T, the subcarrier spacing is $\Delta f = 1/T$, and the subcarriers are located at frequencies

$$f_k = f_c + k/T, \qquad k = -K/2, \ldots, K/2 - 1, \quad (3)$$

where f_c is the center frequency, and K is the total number of subcarriers. Define $\mathcal{S}_A$ and $\mathcal{S}_N$ as the non-overlapping sets of active and null subcarriers respectively, which satisfy $\mathcal{S}_A \cup \mathcal{S}_N = \{-K/2, \ldots, K/2-1\}$. Let $s[k]$ denote the information symbol on the kth subcarrier. The transmitted passband signal is

$$\tilde{x}(t) = 2\text{Re}\left(\sum_{k \in \mathcal{S}_A} s[k] e^{j2\pi f_k t} g(t)\right), \qquad t \in [0, T'], \quad (4)$$

where $T' = (1+\beta)T + T_g$ is the ZP-OFDM block duration accounting for a zero guard time of length T_g; see Fig. 1 for an illustration. The Fourier transform of $\tilde{x}(t)$ for $f > 0$ is

$$\tilde{X}(f) = \sum_{k \in \mathcal{S}_A} s[k] G(f - f_k). \quad (5)$$

Assume that the channel consists of N_p discrete paths

$$h(\tau; t) = \sum_{p=1}^{N_p} A_p(t) \delta(\tau - \tau_p(t)), \quad (6)$$

where $A_p(t)$ and $\tau_p(t)$ are the amplitude and delay of the pth path. Within one OFDM block, we assume that (i) the amplitude does not change $A_p(t) \approx A_p$, and (ii) the path delay can be approximated as

$$\tau_p(t) \approx \tau_p - a_p t,$$

where τ_p is the initial delay and a_p is the Doppler rate of the pth path. The parameter a_p can be expressed as $a_p = v_p/c$, where v_p is the relative speed of the transmitter and the receiver

projected on the pth path, and c is the sound speed in water. As such, the received passband signal is

$$\tilde{y}(t) = \sum_{p=1}^{N_p} A_p \tilde{x}((1+a_p)t - \tau_p) + \tilde{n}(t), \tag{7}$$

where $\tilde{n}(t)$ is the additive noise.

As described in [1], [3], the receiver first performs a resampling operation on the received passband signal to remove the dominant Doppler effect, leading to $\tilde{z}(t) = \tilde{y}\left(t/(1+\hat{a})\right)$ where $(1+\hat{a})$ is the resampling factor; The resampling factor $\hat{a}$ can be estimated based on the packet length change through the use of preamble and postamble [10], or by a synchronization algorithm based on a cyclic-prefixed OFDM preamble [11]. After downshifting, the baseband signal $z(t)$ is often sampled at the baseband rate $K\Delta f$, and hence the sampling interval is T/K. Since null subcarriers are placed at the edges of the signal band, this sampling rate does not incur any information loss. For each ZP-OFDM block, a total of

$$K' \triangleq (1+\beta)K + (T_g/T)K \tag{8}$$

time-domain samples are obtained, which contain all useful information about the current block.

The receivers in [1], [3] first estimate the mean Doppler shift based on the minimization of the energy spilled to null subcarriers [12], [13]. After compensating the mean Doppler shift (say ϵ Hz) on the baseband sequence, FFT operation is performed after overlap-adding. The FFT output on the kth subcarrier can be expressed as

$$\begin{aligned} z[k] &= Z\left(k/T + \epsilon\right) = \tilde{Z}(f_k + \epsilon) \\ &= \tilde{Y}\left((1+\hat{a})(f_k+\epsilon)\right), \quad k = -K/2, \ldots, K/2-1 \end{aligned} \tag{9}$$

where $Z(f)$, $\tilde{Z}(f)$, and $\tilde{Y}(f)$ are the Fourier transforms of $z(t)$, $\tilde{z}(t)$, and $\tilde{y}(t)$, respectively. Channel estimation and symbol detection in [1], [3] are performed based on the K frequency-domain samples $\{z[k]\}_{k=-K/2}^{K/2-1}$.

Clearly, the receivers in [1], [3] do not utilize all the information available per ZP-OFDM block: only K frequently-domain samples are retained while there are $K' > K$ time-domain samples. In this paper, the benefit of frequency-domain oversampling is investigated in the context of underwater acoustic communication systems, and is confirmed using data collected from real experiments.

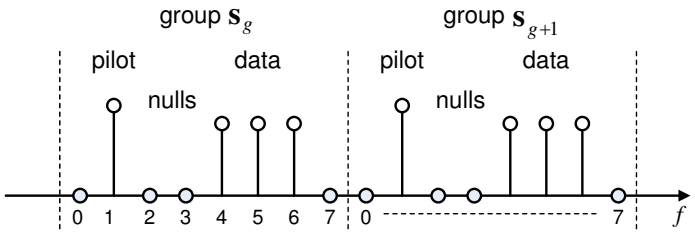

(a) Subcarrier index

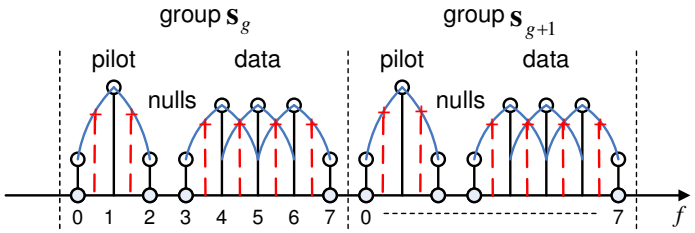

(b) solid lines are samples on the subcarriers, while dashed lines are samples mid-way between consecutive subcarriers.

Fig. 2. The subcarrier index and illustration of oversampling with $\alpha = 2$.

III. The Proposed Transceiver Design

We rely on the signal design in [5], [6], where the data subcarriers are separated from the pilot subcarriers by at least two null subcarriers. Specifically, subcarriers are divided into $N_G \triangleq K/8$ groups, with each group containing 8 subcarriers in the following pattern:

$$\begin{bmatrix} 0 & P & 0 & 0 & D & D & D & 0 \end{bmatrix}, \tag{10}$$

where P and D denote a pilot symbol and a data symbol, respectively; see also Fig. 2. For the gth group, the index for the pilot subcarrier is $p_g = (-K/2) + 8g + 1$, and the indexes for the data subcarriers are $i_g - 1, i_g, i_g + 1$, where $i_g = -(K/2) + 8g + 4$. Some subcarrier groups on the edge of the signal band are turned off.

A. Receiver Model

We next present the channel input-output relationship for the signal design in Fig. 2. Using frequency-domain oversampling with an oversampling factor $\alpha \geq 1$, an αK-point FFT operation is performed after padding $\{\alpha K - K'\}$ zeros to the baseband signal after Doppler shift compensation. Therefore, a total of αK frequency-domain samples are obtained. Obviously, when

$\alpha = 1$, this operation reduces to the overlap-add receiver. Define

$$\check{f}_{m'} = f_c + \frac{m'}{\alpha T}, \qquad m' = -\alpha K/2, \ldots, \alpha K/2 - 1, \tag{11}$$

where m' and k index of the oversampled measurements and the physical subcarriers, respectively. The measurement $z[m']$ on the frequency $\check{f}_{m'}$ can be related to $z(t)$ as [3]

$$z[m'] = \frac{1}{T} \int_0^{(1+\beta)T+T_g} z(t) e^{-j2\pi\epsilon t} e^{-j2\pi \frac{m'}{\alpha T} t} dt. \tag{12}$$

Substituting (4) and (7) into (12) yields,

$$z[m'] = \sum_{p=1}^{N_p} \left[A'_p e^{-j2\pi(\check{f}_{m'}+\epsilon)\tau'_p} \left(\sum_{k \in \mathcal{S}_A} \varrho^{(p)}_{m',k}(b_p) s[k] \right) \right] + \bar{\eta}[m'], \tag{13}$$

where $\bar{\eta}[m']$ is the additive noise and,

$$A'_p = \frac{A_p}{1+b_p}, \qquad \tau'_p = \frac{\tau_p}{1+b_p}, \qquad b_p = \frac{a_p - \hat{a}}{1+\hat{a}}, \tag{14}$$

$$\varrho^{(p)}_{m',k}(b_p) = G\left(\check{f}_{m'} - f_k + \frac{\epsilon - b_p \check{f}_{m'}}{1+b_p} \right). \tag{15}$$

One can find that $(1+b_p)$ represents the residual Doppler rate after the resampling operation,

$$1 + b_p = 1 + \left(\frac{a_p - \hat{a}}{1+\hat{a}} \right) = \frac{1+a_p}{1+\hat{a}}, \tag{16}$$

and A'_p, τ'_p are the scaled amplitude and delay, respectively.

We can rewrite (13) as

$$z[m'] = \sum_{k \in \mathcal{S}_A} \bar{H}_{m',k} s[k] + \bar{\eta}[m'], \tag{17}$$

where $k \in \{-K/2, \ldots, K/2-1\}$ is the subcarrier index, $m' \in \{-\alpha K/2, \ldots, \alpha K/2 - 1\}$ is the index for the FFT outputs, and

$$\bar{H}_{m',k} = \sum_{p=1}^{N_p} A'_p e^{-j2\pi(\check{f}_{m'}+\epsilon)\tau'_p} \varrho^{(p)}_{m',k}(b_p). \tag{18}$$

To separate channel estimation from data detection, we assume that the ICI beyond the direct subcarrier neighbors can be neglected [14]. Specifically, define

$$H_{m',k} = \begin{cases} \bar{H}_{m',k} & |m'/\alpha - k| \leqslant 1 \\ 0 & \text{otherwise} \end{cases}. \tag{19}$$

Eq. (17) can then be rewritten as:

$$z[m'] = \sum_{k \in \mathcal{S}_A} H_{m',k} s[k] + \eta[m']. \tag{20}$$

Clearly, the effective noise is

$$\eta[m'] = \sum_{k \in \mathcal{S}_A} \left(\bar{H}_{m',k} - H_{m',k} \right) s[k] + \bar{\eta}[m']. \tag{21}$$

which consists of the ambient noise and the residual ICI.

B. Sparse Channel Estimation

Based on (20), the receiver draws the following $2\alpha + 1$ frequency-domain samples for each pilot symbol transmitted as

$$\begin{pmatrix} z[\alpha(p_g - 1)] \\ \vdots \\ z[\alpha p_g] \\ \vdots \\ z[\alpha(p_g + 1)] \end{pmatrix} = \begin{pmatrix} H_{\alpha(p_g-1),p_g} \\ \vdots \\ H_{\alpha p_g,p_g} \\ \vdots \\ H_{\alpha(p_g+1),p_g} \end{pmatrix} s[p_g] + \begin{pmatrix} \eta[\alpha(p_g - 1)] \\ \vdots \\ \eta[\alpha p_g] \\ \vdots \\ \eta[\alpha(p_g + 1)] \end{pmatrix}. \tag{22}$$

The channel's frequency response at frequency $\check{f}_{m'}$ can be obtained as

$$\hat{H}_{m',p_g} = z[m']/s[p_g], \qquad m' = \alpha(p_g - 1), \ldots, \alpha(p_g + 1), \tag{23}$$

in which, corresponding to N_G pilot subcarriers, a total of $N_G(2\alpha + 1)$ channel measurements can be collected.

With the limited number of observations, there are much more channel coefficients $\{H_{m',k}\}$ to estimate. Using compressed sensing techniques, the receiver exploits the sparse nature of underwater acoustic channels and jointly estimates the complex gain, Doppler scale, and delay triplets $\{A'_p, b_p, \tau'_p\}_{p=1}^{N_p}$ corresponding to N_p discrete paths. However, this is a *nonlinear* estimation problem, as evidenced by (18). To render the nonlinear estimation problem into a *linear* one, the delay and Doppler scale will be searched over an over-parameterized dictionary, as described next.

Specifically, the sparse channel estimator searches for possible paths on a two dimensional dictionary of (b, τ') of size $N_b \times N_\tau$, with each dimension uniformly discretized as,

$$b \in \{-b_{\max}, -b_{\max} + \Delta b, \ldots, b_{\max}\}, \tag{24}$$

$$\tau' \in \left\{0, \frac{T}{\lambda K}, \frac{2T}{\lambda K}, \ldots, T_g\right\}, \tag{25}$$

where Δb and $T/(\lambda K)$ denote the uniform sampling steps along the delay axis and the Doppler rate axis, respectively, with λ an integer to control the time-domain resolution. Hence, there are $N_b N_\tau$ tentative paths to be searched.

The channel measurements of all the groups can be stacked into an $N_G(2\alpha+1) \times 1$ vector,

$$\hat{\mathbf{h}}_P = [\hat{H}_{\alpha(p_0-1),p_0}, \cdots, \hat{H}_{\alpha(p_0+1),p_0}, \cdots, \hat{H}_{\alpha(p_{N_G}-1),p_{N_G}}, \cdots, \hat{H}_{\alpha(p_{N_G}+1),p_{N_G}}]^T, \tag{26}$$

which shall contain the contributions from all possible paths. Let $\xi_{i,j}$ denote the complex amplitude corresponding to the path on the (b_i, τ_j) grid. Based on (26), (18), (19), one can compactly expressed $\hat{\mathbf{h}}_P$ as

$$\hat{\mathbf{h}}_P = \sum_{i=1}^{N_b}\sum_{j=1}^{N_\tau} \xi_{i,j} \mathbf{\Lambda}_j \mathbf{\Gamma}_i + \boldsymbol{\eta}_P \tag{27}$$

$$= \underbrace{[\mathbf{\Lambda}_1\mathbf{\Gamma}_1, \ldots, \mathbf{\Lambda}_{N_\tau}\mathbf{\Gamma}_{N_D}]}_{:=\mathbf{A}} \underbrace{\begin{pmatrix} \xi_{1,1} \\ \vdots \\ \xi_{N_D,N_\tau} \end{pmatrix}}_{:=\boldsymbol{\xi}} + \boldsymbol{\eta}_P, \tag{28}$$

with $\boldsymbol{\eta}_P$ denoting the channel measurement noise, and

$$\mathbf{\Lambda}_j = \text{diag}\left(e^{-j2\pi(\check{f}_{m'}+\epsilon)\tau'_j}\right),$$

$$[\mathbf{\Gamma}_i]_{m',l} = \begin{cases} \varrho^i_{m',l}(b_i) & |m'/\alpha - l| \leqslant 1 \\ 0 & \text{otherwise} \end{cases},$$

where, $\varrho^i_{m',l}(b_i)$ is defined as in (15), $m' \in \{\alpha(p_g-1), \alpha(p_g-1)+1, \ldots, \alpha(p_g+1)\}_{g=0}^{N_G-1}$ and $l \in \{p_g\}_{g=0}^{N_G-1}$, the sizes of $\mathbf{\Lambda}_j$ and $\mathbf{\Gamma}_i$ are $N_G(2\alpha+1) \times N_G(2\alpha+1)$ and $N_G(2\alpha+1) \times N_G$, respectively.

Noticing that most elements of $\boldsymbol{\xi}$ are zero, the sparse channel parameters are found through the optimization problem,

$$\min_{\boldsymbol{\xi}} \quad \|\hat{\mathbf{h}}_P - \mathbf{A}\boldsymbol{\xi}\|_2 + \zeta|\boldsymbol{\xi}|_1, \tag{29}$$

where the constant ζ controls the sparsity of the solution. In this paper, we use the SpaRSA algorithm from [15] to solve (29).

C. MMSE Channel Equalization

Channel equalization is applied on each group separately. For the gth group with three data symbols $s[i_g-1], s[i_g], s[i_g+1]$, the related channel outputs are

$$\underbrace{\begin{pmatrix} z[\alpha(i_g-2)] \\ \vdots \\ z[\alpha i_g] \\ \vdots \\ z[\alpha(i_g+2)] \end{pmatrix}}_{\triangleq \mathbf{z}_g} = \underbrace{\begin{pmatrix} H_{\alpha(i_g-2),(i_g-1)} & 0 & 0 \\ \vdots & \vdots & \vdots \\ H_{\alpha i_g,(i_g-1)} & H_{\alpha i_g,i_g} & H_{\alpha i_g,(i_g+1)} \\ \vdots & \vdots & \vdots \\ 0 & 0 & H_{\alpha(i_g+2),(i_g+1)} \end{pmatrix}}_{\triangleq \mathbf{H}_g} \underbrace{\begin{pmatrix} s[i_g-1] \\ s[i_g] \\ s[i_g+1] \end{pmatrix}}_{\triangleq \mathbf{d}_g} + \underbrace{\begin{pmatrix} \eta[\alpha(i_g-2)] \\ \vdots \\ \eta[\alpha i_g] \\ \vdots \\ \eta[\alpha(i_g+2)] \end{pmatrix}}_{\triangleq \boldsymbol{\eta}_g} \tag{30}$$

The vector $\mathbf{z}_g$ is of length $4\alpha+1$. With $\alpha = 1$ in the conventional receiver, 5 measurements are used to decode 3 symbols, while an oversampling factor of $\alpha = 2$ leads to 9 available measurements to decode 3 symbols.

Given (21), one can find that the characteristics of $\boldsymbol{\eta}_g$ depend on the ambient noise and the ignored ICI. For simplicity, we assume that $\boldsymbol{\eta}_g$ has zero mean and covariance matrix $N_0\mathbf{I}_{4\alpha+1}$. The MMSE equalizer's output is

$$\hat{\mathbf{d}}_g^{\text{mmse}} = \left(\mathbf{H}_g^H\mathbf{H}_g + \frac{N_0}{E_s}\mathbf{I}_3\right)^{-1}\mathbf{H}_g^H\mathbf{z}_g, \tag{31}$$

where E_s is the symbol energy. In this paper, we estimate the noise variance N_0 based on the energy on the null subcarriers. At high signal-to-noise ratio (SNR), the MMSE equalizer reduces to the zero-forcing (ZF) equalizer given by

$$\hat{\mathbf{d}}_g^{\text{zf}} = \left(\mathbf{H}_g^H\mathbf{H}_g\right)^{-1}\mathbf{H}_g^H\mathbf{z}_g. \tag{32}$$

Other equalizers such as those based on decision feedback (DFE) [7] or Markov Chain Monte Carlo (MCMC) [16], [17] could also be considered. However, since strong nonbinary LDPC channel coding [18] will be used to evaluate the coded block error rate performance, we focus on linear equalizers in this paper.

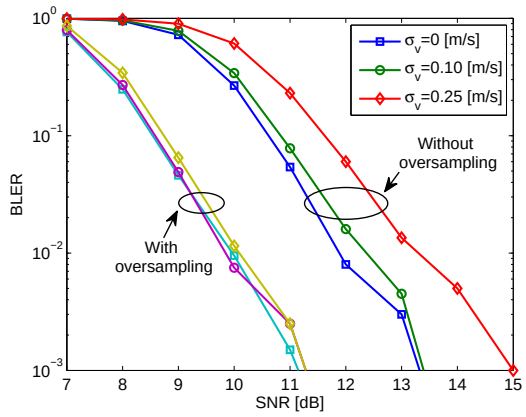

Fig. 3. BLER bound with full channel knowledge, rectangular window

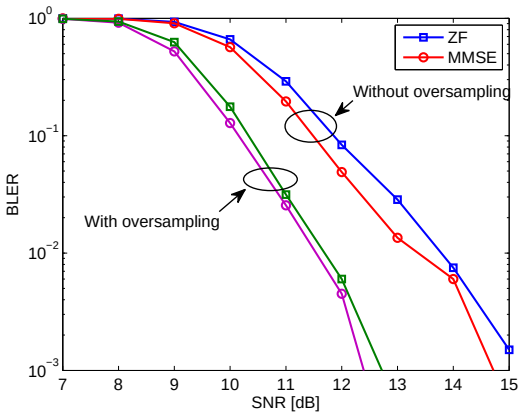

Fig. 4. BLER performance with estimated channels, rectangular window, $\sigma_v = 0.25$ m/s

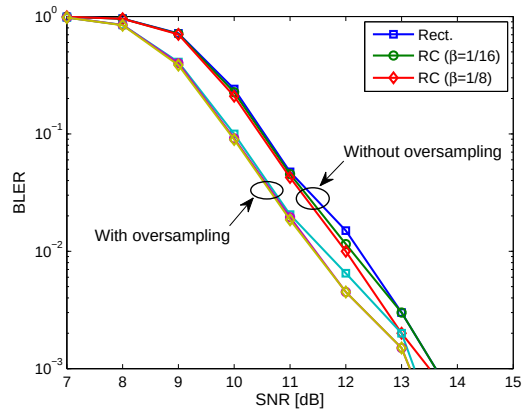

Fig. 5. BLER performance with estimated channels, $\sigma_v = 0.10$ m/s

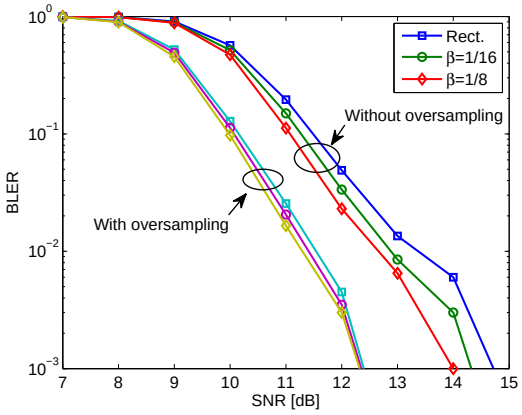

Fig. 6. BLER performance with estimated channels, $\sigma_v = 0.25$ m/s

IV. Numerical Simulation

The sparse channel consists of $N_p = 10$ discrete paths, where the inter-arrival time follows an exponential distribution with mean 0.5 ms. The amplitudes are Rayleigh distributed with the average power decreasing exponentially with the delay, where the difference between the beginning and the end of the guard time of 13.1 ms is 6 dB. The Doppler rate a_p of each path is drawn from a zero mean Gaussian distribution with standard deviation $\sigma_v f_c/c$, where σ_v denotes the standard deviation of the platform velocity, and c is the sound speed in water being set to

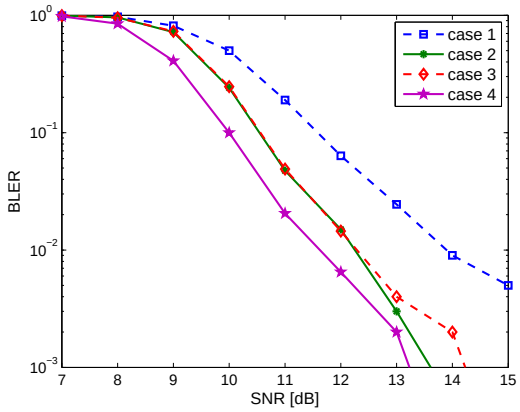

Fig. 7. BLER performance with estimated channels, rectangular window, $\sigma_v = 0.10$ m/s

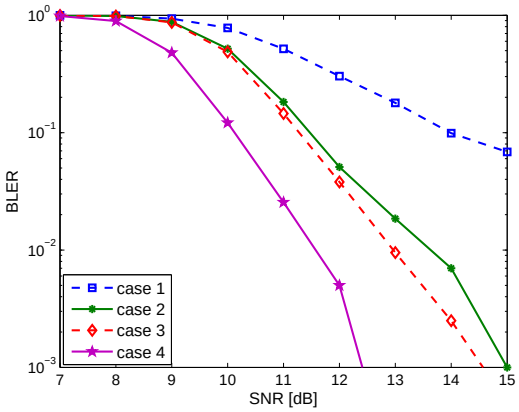

Fig. 8. BLER performance with estimated channels, rectangular window, $\sigma_v = 0.25$ m/s

1500 m/s. Hence, the maximum possible Doppler is about $\sqrt{3}\sigma_v f_c/c$.

The ZP-OFDM signal parameters are tailored according to the setting of the SPACE08 experiment in Table I, with the only exception of $T_g = 13.1$ ms. The subcarrier allocation in Fig. 2 is adopted. Out of the $N_G = K/8 = 128$ groups, 8 groups on each edge of the signal band are turned off for the band protection, while the pilot subcarriers therein are still used to carry pilot symbols. Hence, there are $|\mathcal{S}_P| = 128$ pilot subcarriers and $|\mathcal{S}_D| = 384$ data subcarriers in total. The data symbols are encoded with a rate-$1/2$ nonbinary LDPC code [18] and modulated with a 16-QAM constellation, which leads to data rate:

$$R = \frac{1}{2}\frac{|\mathcal{S}_D| \cdot \log_2 16}{(1+\beta)T + T_g}. \tag{33}$$

For raised-cosine windows with $\beta = 0,\ 1/16,\ 1/8$, the overall data rates are $R = 6.5,\ 6.2,\ 5.9$ kb/s, respectively.

The dictionary for the sparse channel estimation are constructed with $\Delta b = \Delta v/c, \Delta v = 0.06$ m/s, $N_D = 15$ and $\lambda = 2$ in (24) and (25), respectively. The MMSE equalizer of Section III-C is adopted for data symbol detection. The block-error-rate (BLER) after channel decoding is used for the performance comparison.

With full channel knowledge, Fig. 3 demonstrates the BLER performance bound with different standard deviations of the Doppler rate. A total of 2000 Monte Carlo runs are used. Comparing the performance of conventional receiver and the frequency-oversampling receiver, we observe

that the performance of the latter remains almost the same as the Doppler spread increases, while the performance decreases considerably for the receiver without oversampling.

Fig. 4 shows the BLER curves with estimated channel knowledge where both MMSE and zero-forcing (ZF) equalizer are adopted. A total of 2000 Monte Carlo runs are used. One can find that the frequency oversampling receiver outperforms the conventional sampling receiver by about 1.5 dB, while the improvement of MMSE equalizer relative to the ZF equalizer is slight.

Figs. 5 and 6 depict the block-error-rate (BLER) performance of two receivers using different windows and different standard deviations of the Doppler rate. For the conventional sampling receiver, the BLER performance of raised-cosine window is better than that of the rectangular window, and the performance gap improves as the roll-off factor increases. However, for the frequency oversampling receiver, the performance gap between the two types of windows becomes very small. Compared with the windowing operation, the performance gain of the frequency-domain oversampling receiver is more pronounced, especially in the scenario with large velocity deviation.

To understand how much frequency-oversampling helps on different receiver modules, we plot in Figs. 7 and 8 the BLER performance of receivers of four different cases:

- Case 1): conventional sampling for channel estimation and oversampling for data detection;
- Case 2): conventional sampling for both channel estimation and data detection;
- Case 3): oversampling for channel estimation and conventional sampling for data detection;
- Case 4): oversampling for both channel estimation and data detection.

One can find the receiver performance degrades significantly if frequency-domain oversampling is only applied for data symbol detection (case 1), since the channel information at the virtual subcarriers is not explicitly available. The performance of the receiver in case 3 is slightly better than that of the receiver in case 2. Hence, data detection with conventional sampling cannot effectively benefit from the improved channel information due to frequency oversampling. Considerable performance improvement is achieved only when frequency-domain oversampling is used for both channel estimation and data detection.

V. SPACE08 Experimental Results

This experiment was held off the coast of Martha's Vineyard, Massachusetts, from Oct. 14 to Nov. 1, 2008. The water depth was about 15 meters. Among all the six receivers, we only

consider the data collected by three receivers, labeled as S1, S3, S5, which were 60 m, 200 m, and 1000 m away from the transmitter. Each receiver array consists of twelve hydrophones. During the experiment, two storm cycles showed up, one around Julian date 297 and the other around Julian date 300. The latter storm was more severe. We only consider the data recorded from Julian dates 299-301, the days around the second storm cycle. For each day, there are ten recorded files, each consisting of twenty OFDM blocks. Parameter settings of this experiment are summarized in Table I.

TABLE I

OFDM PARAMETERS IN SIMULATION AND SPACE08 EXPERIMENT.

f_c	13 kHz
B	9.77 kHz
K	1024
T	104.86 ms
$\Delta f := 1/T$	9.54 Hz
T_g	24.6 ms

A. BLER Performance with Stationary Receivers

Due to the mild Doppler effect, resampling operation is not performed. One example of the estimated paths on the delay-Doppler plane on Julian date 299 is shown in Fig. 9. The BLER performance averaged over Julian dates 299-301 by combining an increasing number of phones is shown in Fig. 10. Compared with the conventional sampling, frequency-domain oversampling helps to achieve similar performance with less number of phones. Obviously, more frequency-domain observations leads to better channel estimation and symbol detection performance.

B. BLER Performance with Moving Receivers

With the same transmitter, additional data were collected by an 8-element array, towed by a vehicle moving at the speed of about 1 m/s. Four runs of data were collected, each with twenty OFDM blocks. The estimated resampling factor for each run is $[1.0006,\ 0.9991,\ 0.99913,\ 1.0001]$, which corresponds to a moving speed of $[0.85,\ 1.3,\ 1.35,\ 0.15]$ m/s, respectively. One example of the estimated paths on the delay-Doppler plane is shown in Fig. 11. One can see that

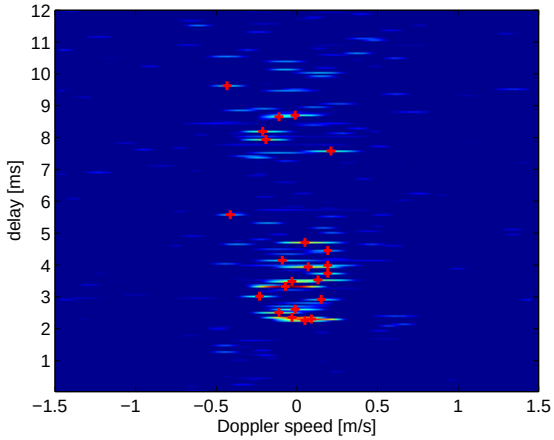

Fig. 9. Sample of sparse channel estimates in the SPACE08 experiment, receiver S3 (1000 m), Julian Data 299.

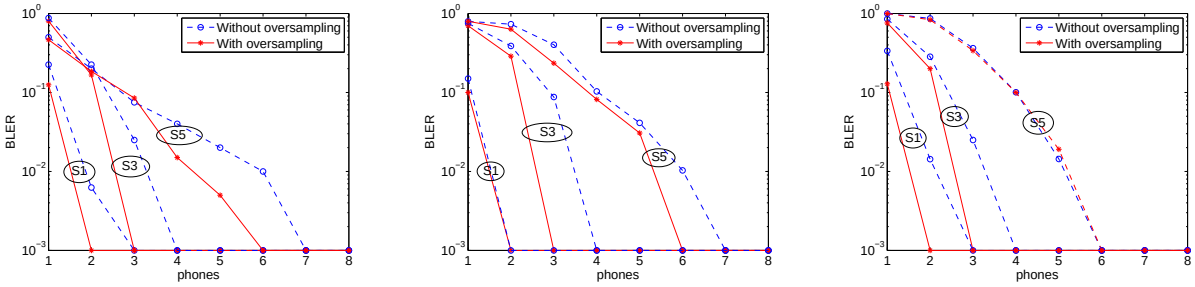

(a) Julian Date 299 (b) Julian Date 300 (c) Julian Date 301

Fig. 10. BLER performance with stationary receivers in the SPACE08 experiment.

the paths are associated with large Doppler rates due to the platform motion. Fig. 12 shows the BLER performance of the conventional sampling method and the frequency oversampling method with and without resampling operation. For the case without resampling operation, the performance gain of frequency oversampling is significant due to the large Doppler scaling effect. After removing the main Doppler effect by resampling the received signal, the performance gap between the conventional sampling method and the frequency oversampling method gets decreased, which agrees very well with the simulation results.

VI. WHOI09 Experimental Results

This experiment was carried out in the Buzzards Bay, Massachusetts, from Dec. 07 to Dec. 08, 2009. The water depth was about 15 meters. Two buoy-based receivers were deployed at 1000 me-

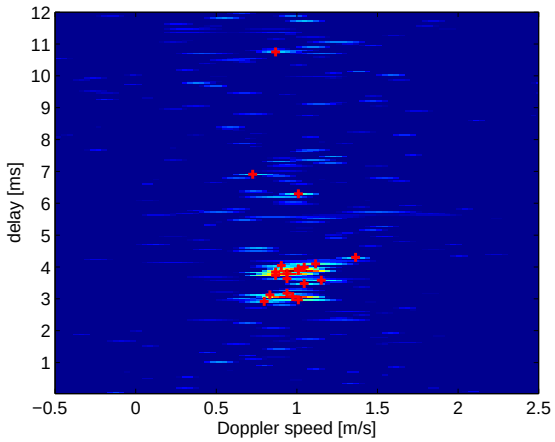

Fig. 11. Sample of sparse channel estimates in the SPACE08 experiment, moving receiver.

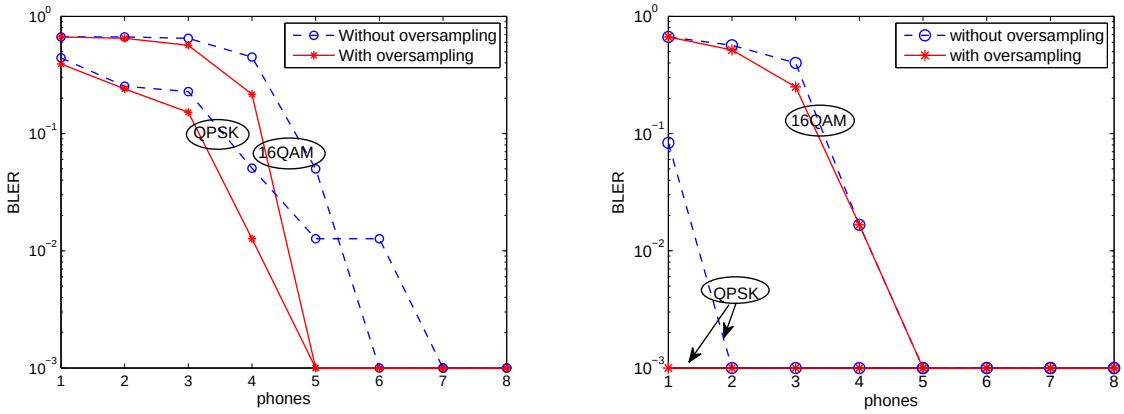

(a) without resampling (b) with resampling

Fig. 12. BLER performance with moving receivers.

ters and 2000 meters away from the transmitter, each with 4 hydrophones. Due to the malfunction of the second hydrophone during the experiment, we only consider the data recorded by the first, third, and fourth phones. There were three transmissions in total, where each transmission consisted of 15 OFDM blocks using the rectangular window, 15 blocks using a raised-cosine window with $\beta = 1/16$, and the other 15 blocks using a raised-cosine window with $\beta = 1/8$. The ZP-OFDM parameters are as follows: $f_c = 31$ kHz, $B = 10$ kHz, $K = 1024$, $T = 102.4$ ms, and $T_g = 24$ ms.

One example of the estimated paths on the delay-Doppler plane is shown in Fig. 13. Due to

the calm environment and large input SNR, most received blocks can be decoded with just one phone, hence, the performance difference between different settings is hard to tell. To enlarge the difference, the received signal is decoded without the Doppler shift compensation step [1]. We here only consider the signal received at the buoy 2000 meters away from the transmitter. The number of decoded blocks in error out of the total 45 blocks are shown in Table II, with 16-QAM constellation and rate-1/2 nonbinary LDPC coding [18]. The benefit of frequency-domain oversampling can be seen.

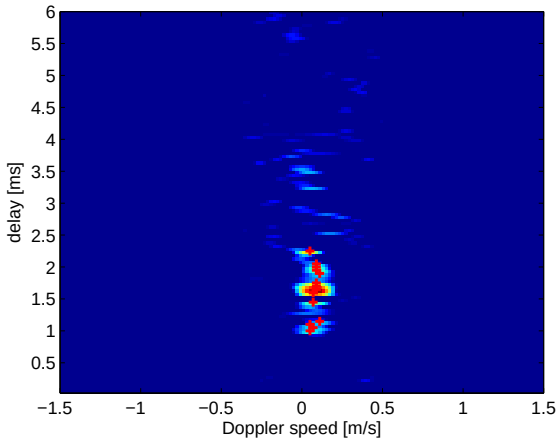

Fig. 13. Sample of sparse channel estimates in the WHOI09 experiment.

TABLE II

THE NUMBER OF DECODED BLOCKS IN ERROR OUT OF 45 BLOCKS; WITHOUT DOPPLER SHIFT COMPENSATION

	The number of Phones	Rectangular window	Raised-cosine $\beta = 1/16$	Raised-cosine $\beta = 1/8$
Without oversampling	1	10	11	6
	2	1	0	1
	3	0	0	0
With oversampling	1	0	0	0
	2	0	0	0
	3	0	0	0

To highlight the performance difference between the window types, the received signal is artificially scaled after main Doppler shift compensation. The scaling factor is chosen according

to a zero mean Gaussian distribution with standard deviation σ_v/c. With 50 Monte Carlo runs, the average BLER curves over the three transmissions (each consisting of 50×15 blocks) versus different standard deviation of the velocity are plotted. Fig. 14 shows the average BLER performance over three transmissions of the scaled version of the received signal with scaling factor of v/c. Compare the BLER performance corresponding to different windows. One can find that the performance using the raised-cosine window is similar to that of rectangular window.

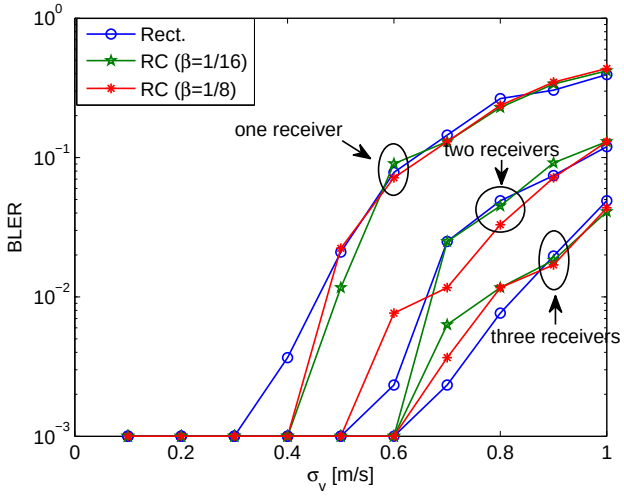

Fig. 14. BLER with conventional sampling, WHOI09 experiment, 16QAM. The received signals are artificially scaled.

VII. Conclusions

In this paper, we presented a zero-padded OFDM transceiver design with rectangular and raised-cosine pulse-shaping windows for underwater acoustic communications. Numerical and experimental results demonstrated that frequency-domain oversampling improves the system performance considerably, and the gain becomes larger as the channel Doppler spread increases.

Acknowledgement

We would like to thank Dr. J. Preisig and his team for conducting the SPACE08 experiment, and Mr. L. Freitag and his team for conducting the WHOI09 experiment.

REFERENCES

[1] B. Li, S. Zhou, M. Stojanovic, L. Freitag, and P. Willett, "Multicarrier communication over underwater acoustic channels with nonuniform Doppler shifts," *IEEE J. Ocean. Eng.*, vol. 33, no. 2, Apr. 2008.

[2] M. Stojanovic, "Low complexity OFDM detector for underwater channels," in *Proc. of MTS/IEEE OCEANS Conf.*, Boston, MA, Sept. 18-21, 2006.

[3] C. R. Berger, S. Zhou, J. Preisig, and P. Willett, "Sparse channel estimation for multicarrier underwater acoustic communication: From subspace methods to compressed sensing," *IEEE Trans. Signal Processing*, vol. 58, no. 3, pp. 1708–1721, Mar. 2010.

[4] B. Muquet, Z. Wang, G. B. Giannakis, M. de Courville, and P. Duhamel, "Cyclic-prefixing or zero-padding for wireless multicarrier transmissions?" *IEEE Trans. Commun.*, vol. 50, no. 12, pp. 2136–2148, Dec. 2002.

[5] S. Mason, C. R. Berger, S. Zhou, K. Ball, L. Freitag, and P. Willett, "An OFDM design for underwater acoustic channels with Doppler spread," in *Proc. of the 2009 DSP & SPE Workshop*, Marco Island, FL, Jan. 2009.

[6] ——, "Receiver comparisons on an OFDM design for Doppler spread channels," in *Proc. of MTS/IEEE OCEANS Conf.*, Bremen, Germany, May 2009.

[7] J. G. Proakis, *Digital Communications*, 4th ed. New York: McGraw-Hill, 2001.

[8] M. Luise, M. Marselli, and R. Reggiannini, "Low-complexity blind carrier frequency recovery for OFDM signals over frequency-selective radio channels," *IEEE Trans. Commun.*, vol. 50, no. 7, pp. 1182–1188, 2002.

[9] Y. R. Zheng, C. Xiao, T. C. Yang, and W.-B. Yang, "Frequency-domain channel estimation and equalization for shallow-water acoustic communications," *Elsevier J. of Physical Commun.*, vol. 3, pp. 48–63, Mar. 2010.

[10] B. S. Sharif, J. Neasham, O. R. Hinton, and A. E. Adams, "A computationally efficient Doppler compensation system for underwater acoustic communications," *IEEE J. Ocean. Eng.*, vol. 25, no. 1, pp. 52–61, Jan. 2000.

[11] S. Mason, C. R. Berger, S. Zhou, and P. Willett, "Detection, synchronization, and Doppler scale estimation with multicarrier waveforms in underwater acoustic communication," *IEEE Journal on Selected Areas in Communications*, vol. 26, no. 9, pp. 1638–1649, Dec. 2008.

[12] H. Liu and U. Tureli, "A high efficiency carrier estimator for OFDM communications," *IEEE Commun. Lett.*, vol. 2, pp. 104–106, Apr. 1998.

[13] X. Ma, C. Tepedelenlioglu, G. B. Giannakis, and S. Barbarossa, "Non-data-aided carrier offset estimations for OFDM with null subcarriers: Identifiability, algorithms, and performance," *IEEE Journal on Selected Areas in Communications*, vol. 19, no. 12, pp. 2504–2515, Dec. 2001.

[14] X. Cai and G. B. Giannakis, "Bounding performance and suppressing intercarrier interference in wireless mobile OFDM," *IEEE Transactions on Communications*, vol. 51, no. 12, pp. 2047–2056, Dec. 2003.

[15] S. J. Wright, R. D. Nowak, and M. A. T. Figueiredo, "Sparse reconstruction by separable approximation," *IEEE Trans. Signal Processing*, vol. 57, no. 7, pp. 2479–2493, Jul. 2009.

[16] B. Farhang-Boroujeny, H. Zhu, and Z. Shi, "Markov chain Monte Carlo algorithms for CDMA and MIMO communication systems," *IEEE Trans. Signal Processing*, vol. 54, no. 5, pp. 1896–1909, May. 2006.

[17] R.-R. Chen, R. Peng, B. Farhang-Beroujeny, and A. Ashikhmin, "Approaching MIMO capacity using bitwise Markov chain Monte Carlo detection," *IEEE Trans. Commun.*, vol. 58, no. 2, pp. 423–428, Feb. 2010.

[18] J. Huang, S. Zhou, and P. Willett, "Nonbinary LDPC coding for multicarrier underwater acoustic communication," *IEEE J. Select. Areas Commun.*, vol. 26, no. 9, pp. 1684–1696, Dec. 2008.